High-*R* Fatigue Crack Growth Threshold Stress Intensity Factors at High Temperatures

Stuart R. Holdsworth and Zhen Chen

Abstract While knowledge relating to the determination and practical application of fatigue crack growth threshold stress intensity factors for defect assessment is relatively well established for many circumstances, this is not the case for materials and conditions which are sensitive to time-dependent mechanisms. There are two well-established international standard procedures for the determination of this fracture mechanics parameter, although their respective crack growth rate criteria differ by an order of magnitude. Unfortunately neither specifically addresses determination of the property for very high-R (K_{min}/K_{max}) ratios, under conditions when the environment can be influential, and ΔK_{th} can be even more sensitive to the da/dN(ΔK) criterion adopted for its determination. In addition to a general state of knowledge review, particular attention is paid to circumstances concerning high-R ΔK_{th} in power plant steels at high temperatures for which oxide-induced crack closure and creep cracking can be influential. Evidence for low-alloy 1%Cr, martensitic 9%Cr and austenitic 17%Cr steels is examined.

Keywords High-R · High temperature · ΔK_{th} · Oxide-induced crack closure Creep cracking

Nomenclature

a	Crack depth
A	Constant in Paris mid-K regime power law
B	Specimen thickness
CT	Compact tension (specimen)
CTOD	Crack opening displacement
da/dN	Fatigue crack growth rate
DCPD	Direct current potential drop (electrical crack monitoring instrumentation)

S. R. Holdsworth (✉) · Z. Chen
Swiss Federal Laboratories for Materials Science and Technology (EMPA),
Uberlandstrasse 129, 8600 Dubendorf, Zurich, Switzerland
e-mail: stuart.holdsworth@empa.ch

R. Prakash et al. (eds.), *Advances in Structural Integrity*,
https://doi.org/10.1007/978-981-10-7197-3_1

f	Frequency
FIB	Focussed ion beam
HCFCG	High-cycle fatigue crack growth (typically for $80 < f < 100$ Hz)
TDFAD	Time-dependent failure assessment diagram
k_p	Oxidation parabolic growth constant
k'	Inelastic strain constant in $\varepsilon(\sigma)$ relationship
K, ΔK	Stress intensity factor, range of stress intensity factor
K_c	Critical stress intensity factor responsible for unstable fracture
K_{mat}^{C}	Material creep toughness (for a given temperature and time)
K_{max}	Maximum stress intensity factor (in cycle)
K_{min}	Minimum stress intensity factor (in cycle)
K_r	K Ratio representing proximity to fracture
ΔK_{th}	Fatigue crack growth threshold stress intensity factor
$d\Delta K_{th}^{ox}$	Enhancement to ΔK_{th} due to oxide-induced crack closure
L_r	Stress ratio representing proximity to plastic collapse or creep rupture
m	Exponent in Paris mid-K regime power law
N	Number of cycles
R	Load ratio (K_{min}/K_{max})
$R_{p0.2}$	0.2% proof strength
R_m	Ultimate tensile strength
R_R	Creep-rupture strength
$R_{0.2}^{C}$	0.2% creep strength (stress responsible for 0.2% inelastic strain for a given temperature and time)
RT	Room temperature
SEM	Scanning electron microscope
t	Time
W	Specimen width
x	Oxide thickness
β	Inelastic strain exponent in $\varepsilon(\sigma)$ relationship
ε, ε_{ref}	Strain, Reference strain
σ, σ_{ref}	Stress, Reference stress
σ_{ref}^{max}	Maximum reference stress (in cycle)
υ	Poisson's ratio

1 Background and Introduction

High-cycle fatigue crack growth (HCFCG) behaviour may conveniently be considered in terms of three regimes, Fig. 1a. These are a low-ΔK regime close to the fatigue crack growth threshold ΔK_{th}, a mid-K regime in which fatigue crack growth rates are represented by a power law [1], and a high-ΔK regime in which da/dN is high and K_{max} approaches the critical stress intensity factor responsible for unstable

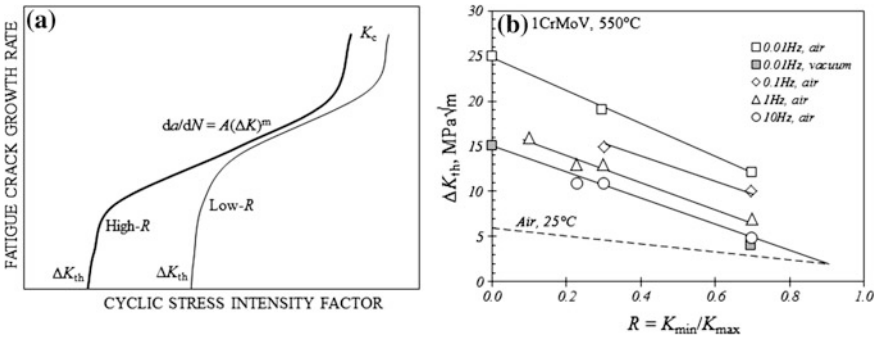

Fig. 1 **a** Schematic representation of high-cycle fatigue crack growth rate characteristics in low-, mid- and high-ΔK regimes; and **b** the influence of frequency, environment and R ratio on fatigue crack growth threshold values for 1CrMoV at 550 °C [2, 5]

fracture, K_c [2]. The focus of the following paper is behaviour in the low-ΔK regime, in particular for high-R (K_{min}/K_{max}) load ratios at high temperatures.

Conceptually, ΔK_{th} is the maximum ΔK associated with no fatigue crack extension. Experimentally, it is assumed to be the ΔK consistent with da/dN 1×10^{-10} m/c [3] or da/dN 1×10^{-11} m/c [4]. At low temperatures, the ΔK_{th} criteria difference may not be important, but this is not the case at high temperatures as will become apparent in the following paper.

In the low-ΔK regime, low da/dN and ΔK_{th} are sensitive to load ratio ($R = K_{min}/K_{max}$), with the magnitude of ΔK_{th} decreasing with increasing R (Fig. 1a). At ambient temperature (RT), higher ΔK_{th} values at low-R are primarily the consequence of plasticity-induced crack closure, but may also be due to contributions from fracture surface roughness-induced closure and fretting oxide-induced closure.

At high temperatures, $\Delta K_{th}(R)$ profiles become increasingly elevated with reducing frequency [2, 5], with the evidence for 1CrMoV steel at 550 °C (which also includes data collected at 0.01 Hz in vacuum), clearly indicating the enhancement of ΔK_{th} to be mainly the consequence of oxide-induced crack closure, Fig. 1b, although plasticity-induced closure is influential at lower R due to lower $R_{p0.2}$ at higher temperatures.

New high-temperature ΔK_{th} results for three steels with different oxidation characteristics (respectively containing 1%Cr, 9%Cr and 17%Cr) have been assessed in terms of fracture surface oxide thickness measurements and a K(CTOD) analysis.

During the course of the study, it became apparent that creep cracking could occur at very low da/dN(ΔK) close to ΔK_{th} under high-R conditions at high temperatures, even for high frequencies not normally expected to be affected by time-dependent cracking processes. A time-dependent failure assessment diagram (TDFAD) approach is adopted to predict the incidence of creep cracking at the tips of very slowly propagating high-R high-cycle fatigue cracks.

2 High-Temperature Fatigue Crack Growth Thresholds

High temperature ΔK_{th} values were determined in accordance with [3] for three steels with different chromium levels, namely 1CrMoV, 9CrMoCo and 17Cr12Ni. As a generality, tests were conducted using compact tension (CT) specimens instrumented with electrical DCPD crack monitoring instrumentation at a frequency (f) of ~80 Hz. Typically, the tests were performed using proportional $W(2B)$ CT specimens with thicknesses (B) of 12.5 or 25 mm. The results determined for a temperature of 550 °C are summarised as a function of R and K_{max} in Fig. 2. The high-temperature values are compared with RT values when available and/or the lower bound RT ΔK_{th} trend line defined in [6].

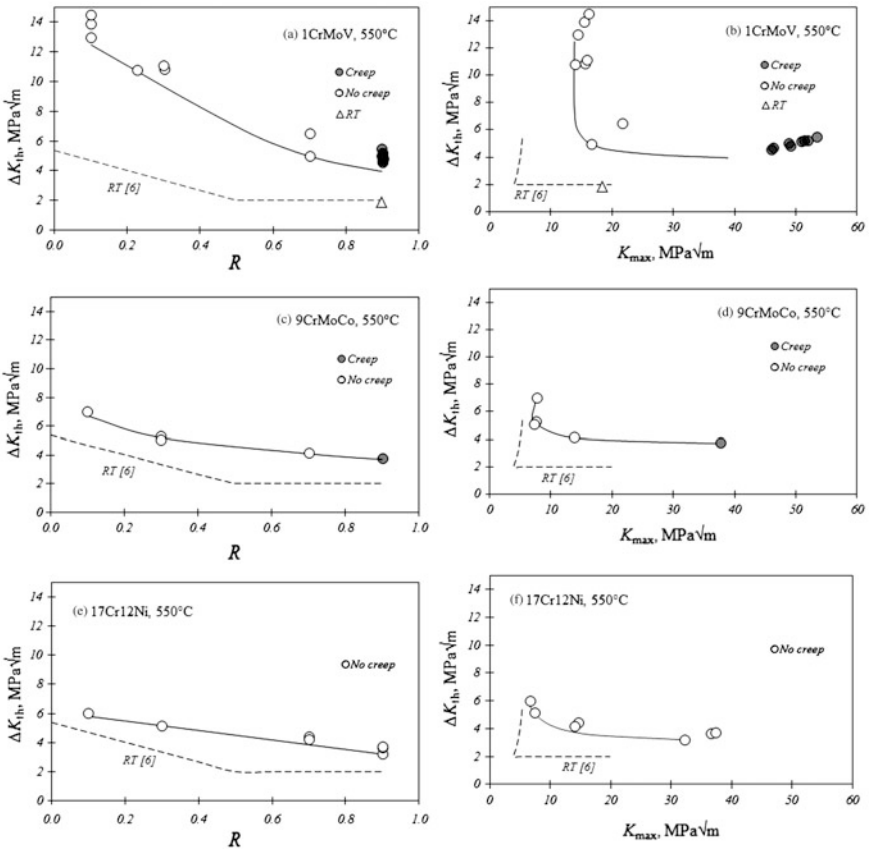

Fig. 2 Variation of ΔK_{th} with R and K_{max}, respectively, at 550 °C for **a**, **b** 1CrMoV, **c**, **d** 9CrMoCo and **e**, **f** 17Cr12Ni (with filled data points representing those tests involving creep crack development when high-cycle fatigue cracking was almost stationary)

As will be considered later, evidence of creep cracking in certain circumstances could be observed at high-R high-cycle fatigue ΔK_{th} test crack tips (when K_{max} and/or σ_{ref}^{max} were high). The filled ΔK_{th} data points in Fig. 2 acknowledge the incidence of creep cracking associated with these tests.

For each steel, there is indication of a ΔK_{th} enhancement, which at high-R can almost exclusively be attributed to oxide-induced crack closure. The extent of high-R ΔK_{th} enhancement ($d\Delta K_{th}^{ox}$) is not the same for each steel (Table 1) and appears to be related to the chromium content. This is examined further in the following section.

3 Oxide-Induced Crack Closure

The growth of oxide scales in air at elevated temperatures on the surfaces of many steels may be predicted with some certainty up to a thickness of ~100 μm by adopting parabolic growth kinetics, i.e.

$$x^2 = k_p.t \tag{1}$$

where upper bound k_p values for 1%Cr, 9%Cr and 17%Cr steels for a temperature of 550 °C are summarised in Table 1 [7]. For oxide thicknesses above ~100 μm, spallation becomes increasingly probable, and adoption of the listed k_p^{UB} values should be with caution. Typically, oxidation kinetics are relatively insensitive to chromium content up to ~10%, above which there is a significant increase in oxidation resistance to ~12%Cr, before a relative stabilization, Fig. 3. The variation in oxidation kinetics is accompanied by the changes in scale formation mechanism shown as insets in Fig. 3 which are likely to be influential in their contribution to $d\Delta K_{th}^{ox}$.

Fracture surface oxide thickness measurements for the three steels were made immediately adjacent to the final crack tips established during ΔK_{th} measurement

Table 1 Summary of oxide-induced crack closure data (550 °C)

Steel	$d\Delta K_{th}^{ox}$ MPa$\sqrt{m}$	k_p^{UB} [7] mm^2/h	$\sqrt{\left(k_p^{UB}t\right)}$ μm	x(FIB) μm	$R_{p0.2}^{550^\circ C}$ MPa	$E^{550^\circ C}$ MPa	K(CTOD) [9] MPa$\sqrt{m}$
1% Cr	2.7	1×10^{-6}	2.5	3.51	445	160,800	2.5
9% Cr	(1.8)	3×10^{-7}	2.7	0.51	483	159,078	1.0
17% Cr	(1.2)	3×10^{-9}	0.5	0.46–1.47	197	165,405	0.4–0.7

$d\Delta K_{th}^{ox}$ values given in parentheses are estimates with reference to the BS7910 RT ΔK_{th} lower bound [6] and are likely to be higher than in practice. NB ΔK_{th} defined in accordance with [3]

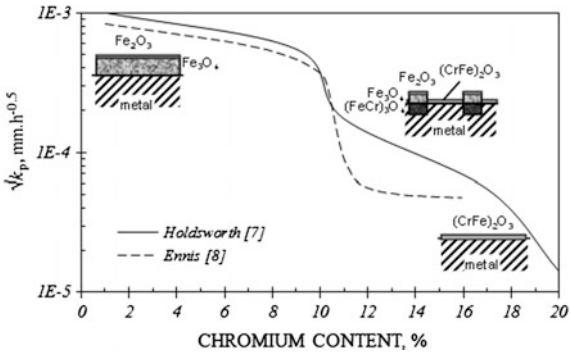

Fig. 3 Variation of oxide growth kinetics with chromium content in steels at 550 °C [8]

campaigns conducted in accordance with [3]. With fracture surface oxide thicknesses being in the range 0.5–3.5 μm as a consequence of being exposed for ~24 h during the final very low d*a*/d*N*(Δ*K*) phase of high-*R* ΔK_{th} determination, an SEM-FIB drilling technique had to be adopted for maximum measurement accuracy. This involved FIB drilling a small trench, typically 1–2 mm deeper than the anticipated oxide scale thickness, with one vertical face and one stepped face. Prior to drilling, a platinum coating was locally sputter-deposited on the fracture surface to provide edge protection and a marker at the position of excavation. Following 'rough' drilling, the ion beam was used to polish the vertical surface of the trench. The sample could then be tilted for oxide thickness measurement directly in the SEM.

Observed FIB-determined oxide thickness measurements compare reasonably well with those calculated using the k_p^{UB} values established in [7], Table 1.

The apparent $d\Delta K_{th}^{ox}$ enhancements experienced by the three steels at 550 °C (Fig. 2) are consistent with the oxide-induced crack closure *K*s which may be predicted using the plane strain Rice relationship [9], i.e.

$$\text{CTOD} = 0.225\left(K/R_{p0.2}\right)^2 \tag{2}$$

The degree of consistency is evident in Table 1 and Fig. 4. An alternative and widely adopted *K*(CTOD) formulation is that proposed by Stewart [10] (Eq. 3), although $d\Delta K_{th}^{ox}$ predictions appear to be excessive using this relationship (Fig. 4).

$$\text{CTOD} = \frac{K^2(1-\upsilon^2)}{2ER_{p0.2}} \tag{3}$$

4 Creep Cracking

An additional mechanism interaction which may be encountered in high-temperature high-*R* ΔK_{th} tests is creep cracking (Fig. 5). Experience has shown that the incidence of creep cracking ahead of very slowly growing

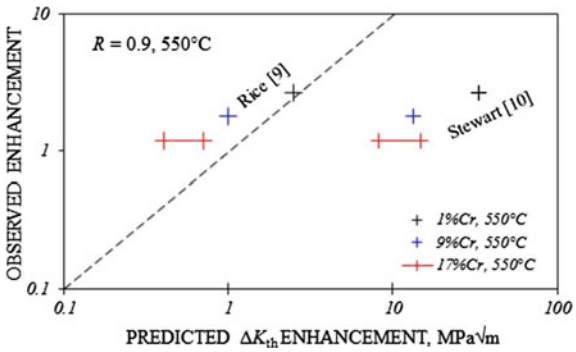

Fig. 4 Comparison of observed $d\Delta K_{th}^{ox}$ for 1%Cr, 9%Cr and 17%Cr steels at 550 °C with predictions based on Rice and Stewart K(CTOD) formulations (respectively, Eqs. 2 and 3)

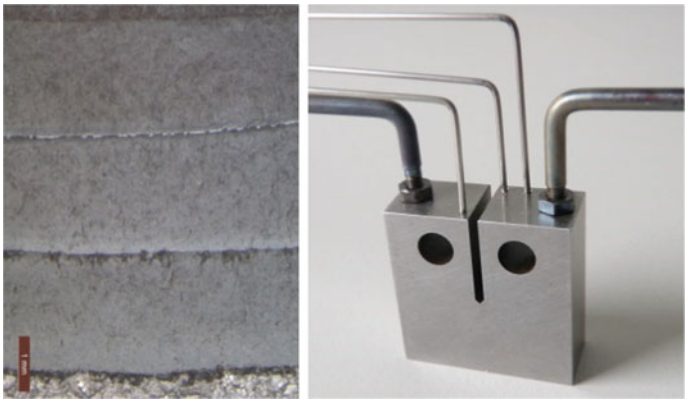

Fig. 5 Evidence of creep cracking (dark bands) at the ends of three high-R ΔK_{th} fatigue cracking campaigns in a $W(2B)12.5$ CT specimen (with inset showing $W(2B)12.5$ CT specimen with DCPD instrumentation attached)

high-cycle fatigue cracks may go undetected by examination only of $da/dN(\Delta K)$ test records. Three additional examples are shown in Fig. 6. Perhaps surprisingly, in these circumstances, fracture surface post-test examination may be the only way to reveal the presence of creep cracking with certainty (e.g. Fig. 6c). However, it is shown that when fracture surface examination is not possible, a TDFAD approach may be adopted to predict the existence of creep cracking when K_{max} approaches K_c^{mat} and/or σ_{ref} approaches $R_{0.2}^{C}$.

While there are two types of high-temperature failure assessment diagram [11], the one favoured for this application is the R5 TDFAD construction [12]. The failure envelope for this diagram is defined by:

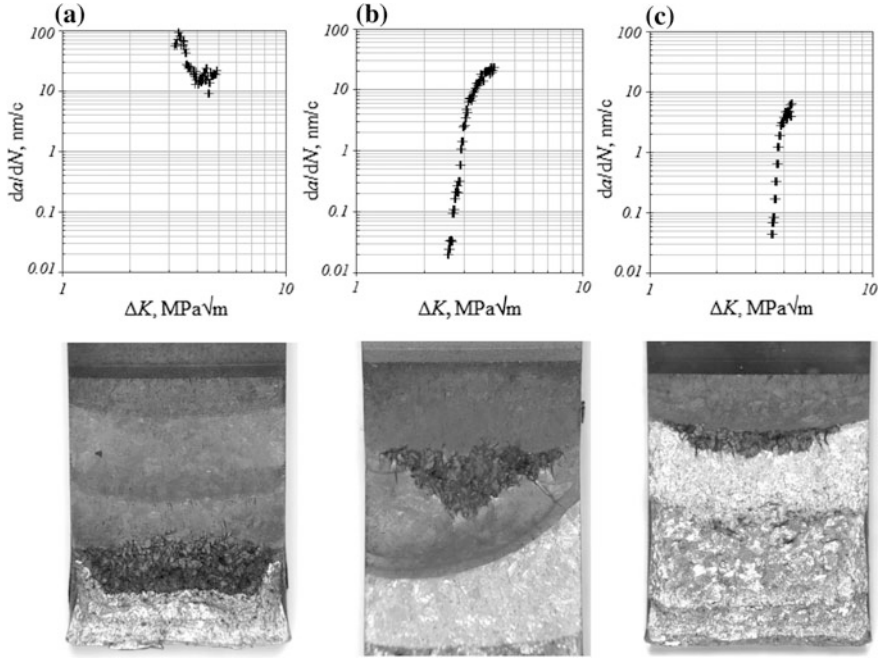

Fig. 6 Examples of high-R high-cycle da/dN(ΔK) records (with accompanying post-test fracture surfaces) for ΔK_{th} tests during which creep cracking has occurred with; **a** expected da/dN(ΔK) response, **b** a discernible but unexpected da/dN(ΔK) response and **c** a hardly discernible da/dN (ΔK) response ($W(2B)$12.5 CT specimens are 12.5 mm thick)

Table 2 Summary of TDFAD material parameter data (550 °C)

Steel	k'	β	K^{C}_{mat} MPa$\sqrt{m}$	$R^{C}_{0.2}$ MPa
1%Cr	730	9	48	366
9%Cr	1200	5	42	345
17%Cr	331.9	11.4	130	123

$$K_r = \left[\frac{E\varepsilon_{ref}}{L_r R^{C}_{0.2}} + \frac{(L_r)^3 R^{C}_{0.2}}{2E\varepsilon_{ref}}\right] \quad \text{for } L_r \le L_r^{max} \tag{4}$$

$$K_r = 0 \quad \text{for } L_r > L_r^{max}$$

where $K_r = K/K^{C}_{mat}$, $L_r = \sigma_{ref}/R^{C}_{0.2}$ and $L_r^{max} = R_R/R^{C}_{0.2}$. The parameters used for TDFAD construction for the three steels considered in this study at 550 °C are summarised in Table 2.

Important information for construction of the TDFAD envelope (Eq. 4) is isochronous $\varepsilon(\sigma, t)$ data for the time period of interest. Typically, for ΔK_{th} tests involving an ASTM da/dN(ΔK) criteria [3], high-cycle fatigue cracks can be almost

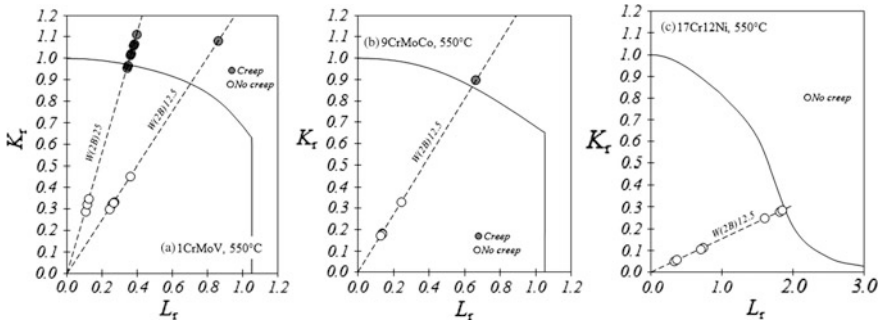

Fig. 7 TDFAD constructions for 1CrMoV, 9CrMoC and 17Cr12Ni steels at 550 °C (with filled data points representing those tests involving creep crack development when high-cycle fatigue cracking was almost stationary)

stationary for ~24 h, and $\varepsilon(\sigma)$ for this period are modelled from data from various sources (e.g. [11, 13]), Table 2, using:

$$\varepsilon = \frac{\sigma}{E} + \left(\frac{\sigma}{k'}\right)^{\beta} \tag{5}$$

TDFADs for the three steels at 550 °C are given in Fig. 7. As in Fig. 2, filled co-ordinates are used to represent those high-*R* ΔK_{th} tests involving creep crack development when high-cycle fatigue cracking is almost stationary. The TDFAD envelope acceptably predicts creep crack development in high-*R* ΔK_{th} tests for the 1CrMoV and 9CrMoCo steels at 550 °C. There is not yet the same evidence for 17Cr12Ni in Fig. 7, primarily because 550 °C is low in the creep range for this steel.

5 Practical Implications

5.1 da/dN(ΔK_{th}) Criterion Sensitivity: Oxidation

It has already been acknowledged that there are two international standards covering the determination of ΔK_{th} with very different d*a*/d*N* criteria defining fatigue crack growth threshold stress intensity factor. The ΔK_{th} d*a*/d*N* criterion in the ASTM standard is 1×10^{-10} m/c [3], whereas that in the ISO standard is 1×10^{-11} m/c [4].

While this anomaly is unlikely to have a big influence at low temperatures for materials tested in what for them are relatively inert conditions, the evidence indicates that the situation is very different at high temperatures.

Depending on the oxidation resistance of a material at a given temperature, ΔK_{th} can be significantly enhanced as a consequence of oxide-induced crack closure. For example, for a ΔK_{th} d*a*/d*N* criterion of 1×10^{-10} m/c, high-cycle fatigue cracking

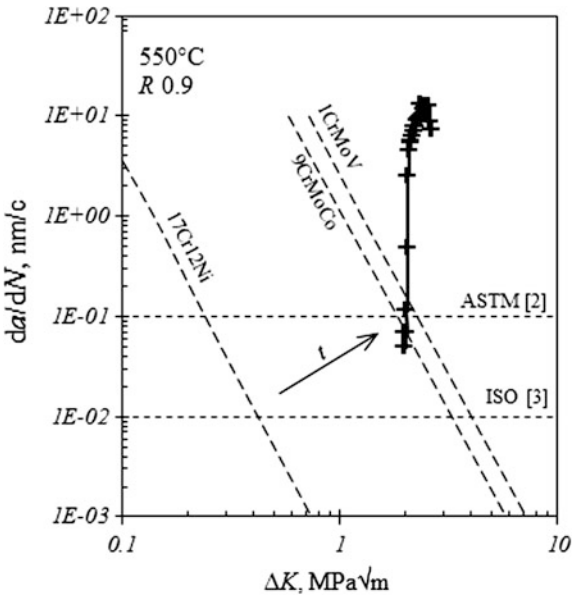

Fig. 8 Influence of time (oxidation) on $da/dN(d\Delta K_{th}^{ox})$ (diagonal broken lines for three steels) and ultimately on material independent high-R $da/dN(\Delta K)$ (connected black crosses), and the consequence of different ΔK_{th} da/dN criteria [3, 4] (for crack size resolution of 0.25 mm [3])

can be close to stationary for ~24 h, and $d\Delta K_{th}^{ox}$ is ~2.7 MPa$\sqrt{m}$ for 1CrMoV at 550 °C (Table 1). For a ΔK_{th} da/dN criterion of 1×10^{-11} m/c, high-cycle fatigue cracking may be close to stationary for >100 h, and, in these circumstances, $d\Delta K_{th}^{ox}$ could be >4 MPa$\sqrt{m}$ for 1CrMoV at 550 °C (i.e. with $\Delta K_{th} > 6$ MPa$\sqrt{m}$ for $R = 0.9$).

The situation is illustrated in Fig. 8. This shows a relatively material independent reducing high-R $da/dN(\Delta K)$ record representative of time insensitive conditions (connected black crosses). It also shows three diagonal iso-da/f $da/dN(d\Delta K_{th}^{ox})$ lines (one for each of the Cr steels) representing crack size resolution (~0.25 mm [3]) and minimum test times (with the iso-da/f $da/dN(d\Delta K_{th}^{ox})$ reference lines being determined by substituting $dt = da(dN/da)/f$ into Eq. 2).

With longer test times at temperature, the diagonal $da/dN(d\Delta K_{th}^{ox})$ lines move towards the right (Fig. 8). The consequence of this is enhanced ΔK_{th} values. Importantly, if the adopted ΔK_{th} test ΔK reduction rates are slower than the oxidation rates, $da/dN(\Delta K)$ can be prevented from reducing to the standard defined ΔK_{th} da/dN criteria.

5.2 *da/dN(ΔK$_{th}$) Criterion Sensitivity:* Creep Cracking

The evidence in Fig. 7 indicates that, while it could have been possible to predict the incidence of creep cracking during high-R ΔK_{th} determinations for the 1CrMoV steel with only a knowledge of K_{mat}^{C}, it would not for the 9%Cr and in 17%Cr steels, for which a TDFAD analysis is required.

6 Concluding Remarks

High-*R* high-cycle fatigue crack growth thresholds for power plant steels are enhanced at high temperatures due to oxide-induced crack closure.

The extent of any enhancement of ΔK_{th} due to oxide-induced crack closure depends on time at low d*a*/d*N*, temperature and material/oxidation mechanism. Consequently, the adopted standard defined d*a*/d*N*(ΔK_{th}) criterion becomes increasingly important with increasing temperature.

High-*R* ΔK_{th} values are increasingly influenced by the development of creep cracking at very low d*a*/d*N* with increasing temperature. While this may only be possible to detect with certainty by fracture surface examination, evidence is presented to show that creep cracking in these circumstances may be predicted using a TDFAD analysis.

References

1. P.C. Paris, F. Erdogan, A critical examination of crack propagation laws. J. Basic Eng. **85**(4), 528–533 (1963)
2. S.R. Holdsworth, in *High Temperature Fatigue Crack Growth*, ed. by J.B. Marriott. High Temperature Crack Growth in Steam Turbine Materials, (Commission European Communities, COST Monograph EUR 14678EN, 1994), pp. 129–176
3. E 647, *in Standard Test Method for Measurement of Fatigue Crack Growth Rates*, (ASTM Standard, ASTM International, West Conshohocken, PA, US)
4. ISO 12108, *in Metallic Materials—Fatigue Testing—Fatigue Crack Growth Method*, International Standard
5. R.P. Skelton, J.R. Haigh, Fatigue crack growth rates and thresholds in steels under oxidising conditions. Mat. Sci. Eng. **36**, 17–25 (1978)
6. BS 7910, *in Guide to Methods for Assessing the Acceptability of Flaws in Metallic Structures*, (British Standards Institution, 2013)
7. S.R. Holdsworth, in *Review of Air Oxidation Kinetics for a Range of Low and High Alloy Steels*, unpublished (2000)
8. P.J. Ennis, W.J. Quadakkers, Mechanisms of steam oxidation in high strength martensitic steels. Int. J. Pres. Ves. Pip. **84**, 75–81 (2007)
9. J.R. Rice, in *The Mechanics of Crack Tip Deformation and Extension by Fatigue*. Fatigue Crack Propagation, vol. 415 (ASTM STP 1967), pp. 247–311
10. A.T. Stewart, The influence of environment and stress ratio on fatigue crack growth at near threshold stress intensities in low alloy steels. Eng. Fract. Mech. **13**(3), 463–478 (1980)
11. D.W. Dean, R.D. Patel, A. Klenk, F. Mueller, Comparison of procedures for the assessment of creep crack initiation. OMMI **3**(3), (2004)
12. R5, An Assessment Procedure for the High Temperature Response of Structures, EDF Energy, 3 (2003)
13. ASME, in *Boiler and Pressure Vessel Code III, Rules for construction of nuclear facility components, Class 1 components in elevated temperature service, Division 1—Subsection NH*, ASME (2004)